AMERICAN SOCIETY FOR MICROBIOLOGY | Journal of Virology

# Activation of RNase L by Murine Coronavirus in Myeloid Cells Is Dependent on Basal *Oas* Gene Expression and Independent of Virus-Induced Interferon

L. Dillon Birdwell,[a] Zachary B. Zalinger,[a] Yize Li,[a] Patrick W. Wright,[b] Ruth Elliott,[a] Kristine M. Rose,[a]* Robert H. Silverman,[c] Susan R. Weiss[a]

Department of Microbiology, Perelman School of Medicine, University of Pennsylvania, Philadelphia, Pennsylvania, USA[a]; Department of Biomedical Engineering, Washington University in St. Louis, St. Louis, Missouri, USA[b] and Department of Cancer Biology, Cleveland Clinic, Cleveland, Ohio, USA[c]

## ABSTRACT

**The oligoadenylate synthetase (OAS)-RNase L pathway is a potent interferon (IFN)-induced antiviral activity. Upon sensing double-stranded RNA, OAS produces 2′,5′-oligoadenylates (2-5A), which activate RNase L. Murine coronavirus (mouse hepatitis virus [MHV]) nonstructural protein 2 (ns2) is a 2′,5′-phosphodiesterase (PDE) that cleaves 2-5A, thereby antagonizing RNase L activation. PDE activity is required for robust replication in myeloid cells, as a mutant of MHV (ns2$^{H126R}$) encoding an inactive PDE fails to antagonize RNase L activation and replicates poorly in bone marrow-derived macrophages (BMM), while ns2$^{H126R}$ replicates to high titer in several types of nonmyeloid cells, as well as in IFN receptor-deficient (*Ifnar1*$^{-/-}$) BMM. We reported previously that myeloid cells express significantly higher basal levels of OAS transcripts than nonmyeloid cells. Here, we investigated the contributions of *Oas* gene expression, basal IFN signaling, and virus-induced IFN to RNase L activation. Infection with ns2$^{H126R}$ activated RNase L in *Ifih1*$^{-/-}$ BMM to a similar extent as in wild-type (WT) BMM, despite the lack of IFN induction in the absence of MDA5 expression. However, ns2$^{H126R}$ failed to induce RNase L activation in BMM treated with IFNAR1-blocking antibody, as well as in *Ifnar1*$^{-/-}$ BMM, both expressing low basal levels of *Oas* genes. Thus, activation of RNase L does not require virus-induced IFN but rather correlates with adequate levels of basal *Oas* gene expression, maintained by basal IFN signaling. Finally, overexpression of RNase L is not sufficient to compensate for inadequate basal OAS levels.**

## IMPORTANCE

**The oligoadenylate synthetase (OAS)-RNase L pathway is a potent antiviral activity. Activation of RNase L during murine coronavirus (mouse hepatitis virus [MHV]) infection of myeloid cells correlates with high basal *Oas* gene expression and is independent of virus-induced interferon secretion. Thus, our data suggest that cells with high basal *Oas* gene expression levels can activate RNase L and thereby inhibit virus replication early in infection upon exposure to viral double-stranded RNA (dsRNA) before the induction of interferon and prior to transcription of interferon-stimulated antiviral genes. These findings challenge the notion that activation of the OAS-RNase L pathway requires virus to induce type I IFN, which in turn upregulates OAS gene expression, as well as to provide dsRNA to activate OAS. Our data further suggest that myeloid cells may serve as sentinels to restrict viral replication, thus protecting other cell types from infection.**

The coronavirus mouse hepatitis virus (MHV) strain A59 (referred to here as A59) causes moderate hepatitis and mild encephalitis, followed by chronic demyelinating disease, in susceptible C57BL/6 (B6) mice (1–3). A59 is cleared from the liver and central nervous system (CNS) primarily by the T cell response 7 to 10 days postinfection (4, 5). However, type I interferon (IFN) production, an early innate immune response, is crucial for early control of MHV infection, as mice deficient in type I IFN receptor expression (*Ifnar1*$^{-/-}$) uniformly die by 2 days after infection (6–8). Interestingly, A59 fails to induce IFN-α/β in most cell types, with the notable exception of myeloid cells (7). Induction of IFN-α/β in macrophages and brain-resident microglia during MHV infection is dependent on sensing of viral double-stranded RNA (dsRNA) by the cytosolic RNA helicase melanoma differentiation-associated gene 5 (MDA5), encoded by *Ifih1* (7, 9, 10). IFN induces a large array of interferon-stimulated genes (ISGs), which include pattern recognition receptors (PRRs), signaling molecules, transcription factors, and antiviral effectors (11–16) (Fig. 1, left, diagrams IFN synthesis and signaling in MHV-infected macrophages). The only other source of type I IFN during A59 infection, primarily IFN-α, is induced through a TLR7-dependent pathway in plasmacytoid dendritic cells (pDCs) (17).

Among the ISGs are several *Oas* genes encoding proteins that function as nucleic acid sensors to synthesize 2′,5′-oligoadenylates (2-5A) in response to viral dsRNA in the host cytosol (18). Mice express several oligoadenylate synthetase (OAS) proteins that produce 2-5A, including OAS1a/g, OAS2, and OAS3, as well

**Received** 2 December 2015 **Accepted** 30 December 2015

**Accepted manuscript posted online** 6 January 2016

**Citation** Birdwell LD, Zalinger ZB, Li Y, Wright PW, Elliott R, Rose KM, Silverman RH, Weiss SR. 2016. Activation of RNase L by murine coronavirus in myeloid cells is dependent on basal *Oas* gene expression and independent of virus-induced interferon. J Virol 90:3160–3172. doi:10.1128/JVI.03036-15.

**Editor:** S. Perlman

Address correspondence to: Susan R. Weiss, weisssr@upenn.edu.

* Present address: Kristine M. Rose, PATH, 455 Massachusetts Avenue NW, Suite 1000, Washington, DC, USA.

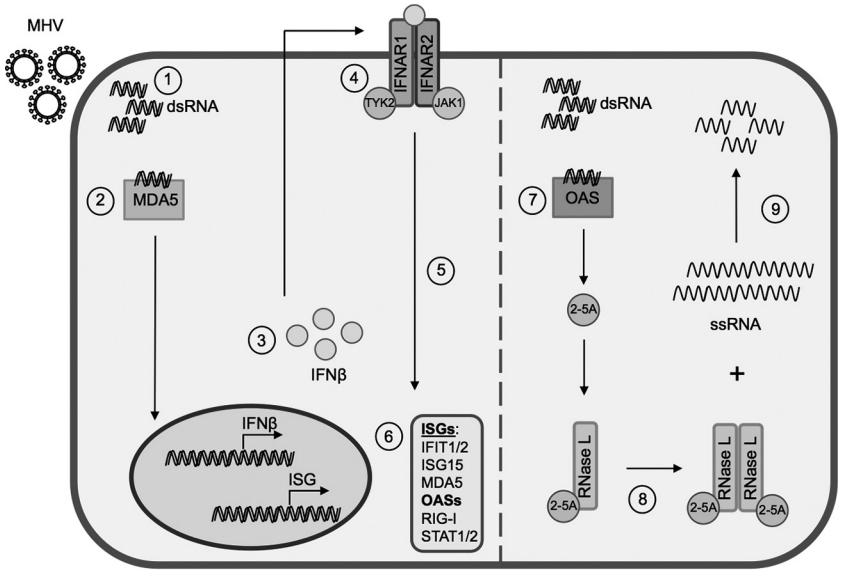


**FIG 1** OAS-RNase L pathway. (Left) Interferon induction and signaling. Viral dsRNA is produced during virus replication (1) and sensed by PRRs, such as MDA5 (2), initiating a signaling pathway leading to transcription, translation, and secretion of IFN-α/β (3). Autocrine and paracrine IFN signaling through the interferon receptor (IFNAR1) (4) stimulates the expression of ISGs (5 and 6). (Right) RNase L activation. (7) OASs sense viral dsRNA and synthesize 2-5A. (8) 2-5A binds to RNase L, inducing its dimerization and subsequent activation. (9) RNase L degrades RNA.

as OASL2 (19–21). The 2-5A binds to and activates latent RNase L by inducing conformational changes and subsequent dimerization (11, 13, 22). RNase L activation leads to restriction of virus replication through the degradation of host and viral single-stranded RNAs, inhibition of protein synthesis, and finally apoptosis (14, 23, 24) (Fig. 1, right, diagrams the activation of RNase L).

Interactions of viruses with the OAS-RNase L pathway are complex. Many viruses encode proteins that inhibit this pathway to various extents, underscoring the significance of the system in restricting viral propagation (13, 25–28). Among the most potent of these inhibitors is the A59 accessory protein, nonstructural protein 2 (ns2), a 2′,5′-phosphodiesterase (PDE) that cleaves 2-5A, thereby preventing RNase L activation (25). An A59 mutant ($ns2^{H126R}$) expressing an inactive PDE (due to an H126R substitution of a catalytic histidine residue) fails to effectively antagonize RNase L and consequently is attenuated for replication in myeloid cells and in the livers of mice (25).

We have found that RNase L activation is most robust in myeloid lineage cells, where basal *Oas* gene expression levels are highest compared with several other types of nonmyeloid primary cells, including astrocytes, neurons, and oligodendrocytes, as well as transformed cell lines (29). Constitutive, low-level type I IFN production in the absence of infection maintains basal levels of expression of ISGs, including OAS (30, 31). It has been generally accepted that RNase L activation requires viral infection both to induce type I IFN production, which in turn upregulates OAS gene expression, and to provide dsRNA for activation of OAS to produce 2-5A (13). Thus, unlike most other IFN-induced activities, which can be stimulated in uninfected cells by paracrine IFN exposure, RNase L can be activated only in infected cells.

To further elucidate the cell-type-dependent determinants of RNase L activation, we investigated basal *Oas* mRNA expression, basal IFN signaling, and viral induction of IFN as three potential contributors. Our data indicate that RNase L activation depends on relatively high basal mRNA expression levels of *Oas* genes typical of myeloid cells and that overexpression of RNase L is not sufficient to overcome insufficient levels of OAS. Furthermore, RNase L activation requires adequate basal IFN signaling to maintain basal *Oas* mRNA expression. However, in contrast to the current paradigm, RNase L activation does not require IFN induction during virus infection of macrophages. These data suggest that myeloid cells can activate RNase L early during infection and before the induction of IFN and thereby limit viral spread to other cell types.

## MATERIALS AND METHODS

**Viruses, cell lines, and mice.** Murine L2 fibroblasts were maintained in Dulbecco's modified Eagle's medium (DMEM) supplemented with 10% fetal bovine serum (FBS), HEPES (10 mM), and 1% penicillin-streptomycin. Plaque assays were performed on L2 cells as described previously (32). Murine 3T3/pLZ fibroblasts and control 3T3/neo (33) cells were grown in DMEM containing 10% FBS supplemented with G418 (350 μg/ml) and 1% penicillin-streptomycin. The recombinant coronaviruses inf-MHV-A59 (wild-type [WT] A59, referred to as A59 here) and inf-ns2-H126R (referred to as $ns2^{H126R}$ here) were obtained from Stuart Siddell (University of Bristol, Bristol, United Kingdom) and have been described previously (2, 34). Newcastle disease virus expressing green fluorescent protein (NDV-GFP) (7, 29, 35) was obtained from Luis Martinez-Sobrido (University of Rochester School of Medicine). B6 mice were purchased from the National Cancer Institute (Frederick, MD). *Rnasel*$^{-/-}$ mice (bred for 10 generations to obtain a B6 background) were described previously (14). *Ifih1*$^{-/-}$ (36) and *Ifnar1*$^{-/-}$ (37) mice, both with B6 background, were obtained from Michael S. Diamond (Washington University in St. Louis, St. Louis, MO). Both strains were further bred and maintained in the animal facility at the University of Pennsylvania, Philadelphia, PA.

**qRT-PCR.** RNA was isolated with an RNeasy minikit (Qiagen, Valencia, CA). Quantitative real-time reverse transcriptase (qRT)-PCR was performed as described previously (2). Briefly, 200 ng (cells) or 350 ng (tissue) of total RNA was reverse transcribed into cDNA using reverse transcriptase (Superscript III; Invitrogen) in a total volume of 20 μl. Then,

2 μl of cDNA was combined with 12.5 μl of iQ5 SYBR green mix (Bio-Rad, Hercules, CA), 6.5 μl diethyl pyrocarbonate (DEPC)-treated water, and 4 μl primer mix (5 μM each). DNA was amplified using an iQ5 iCycler (Bio-Rad), and cycle threshold ($C_T$) values were recorded. Expression levels of mRNA were quantified as $\Delta C_T$ values relative to β-actin mRNA and expressed as $2^{-\Delta CT}$, where $\Delta C_T$ is equal to $C_{T\,\text{Target Gene}}$ minus $C_{T\,\beta\text{-actin}}$. Quantitative RT-PCR primer sequences are available upon request.

**Primary cell cultures. (i) BMM.** Bone marrow-derived macrophages (BMM) were generated from the hind limbs of B6 (WT), *Ifih1*$^{-/-}$, or *Ifnar1*$^{-/-}$ mice as described previously (25, 38, 39) and cultured in DMEM supplemented with 10% FBS and 30% L929 cell-conditioned medium for 6 days before infection. Cultures were routinely ≥99% pure, as assessed by positive staining for expression of CD11b and negative staining for expression of CD11c.

**(ii) BMDC.** Bone marrow-derived dendritic cells (BMDC) were generated from the hind limbs of WT mice as described previously (40, 41) and cultured in RPMI 1640 (Sigma-Aldrich) supplemented with 10% FBS, 2 mM L-glutamine, 1% penicillin-streptomycin, 50 μM β-mercaptoethanol, and 20 ng/ml of granulocyte-macrophage colony-stimulating factor (GM-CSF) (Peprotech). The cells were fed on days 3, 6, and 8 with fresh medium and supplements. On day 10, cells were harvested and replated at 200,000 cells/well using growth medium with 5 ng/ml GM-CSF on 24-well non-tissue-culture-treated plates and used for infections. Cells were routinely >95% CD11c$^+$ and 80 to 90% immature (major histocompatibility complex class II low [MHC-II$^{lo}$]).

**(iii) Hippocampal neurons.** Hippocampal neurons were prepared from embryonic day 15.5 (E15.5) (E15 to E16) mouse embryos as described previously (42). Briefly, cells were seeded onto poly-L-lysine-coated tissue culture plates; cultured in neurobasal medium containing B-27 supplement (Invitrogen), 1% penicillin-streptomycin, 2 mM L-glutamine, and 4 μg/ml glutamate for 4 days in the absence of an astrocyte feeder layer; and then used for infections. Neuron cultures were routinely 95 to 98% pure, as determined by positive immunostaining for MAP2 and negative immunostaining for CD11b (microglia-specific marker), glial fibrillary acidic protein (GFAP) (astrocyte-specific marker), and OLIG2 (oligodendrocyte-specific marker) (42).

**(iv) Mixed glial cultures.** (iv) Mixed glial cultures, consisting of astrocytes and microglia, were generated from the brains of 1- to 3-day-old neonatal mice as described previously (25). Briefly, tissue was dissociated by mechanical disruption through a 70-μm nylon mesh filter; plated in complete medium consisting of DMEM supplemented with 10% FBS, 1% nonessential amino acid solution, 2 mM L-glutamine, 1% penicillin-streptomycin, and 10 mM HEPES; and cultured for 9 to 11 days. These cells were lifted from their culture vessel using enzyme-free Hanks' balanced salt solution-based cell disassociation buffer (Gibco).

**(v) Astrocytes.** (v) Astrocyte cultures were generated as described for mixed glial cultures, and after 9 to 11 days in culture, the flasks were shaken to remove nonadherent microglial cells; the remaining adherent cells were ≥95% pure astrocytes, as determined by positive immunostaining for GFAP (25), and were used for infection. The protocols were approved by the Institutional Animal Care and Use Committee at the University of Pennsylvania.

**Infections of cell cultures.** Virus was added to cells at a multiplicity of infection (MOI) of 1 PFU/cell and allowed to adsorb for 1 h at 37°C. The cultures were washed with PBS (3 times) and fed with medium as described for each cell type. The culture supernatants were harvested at the times indicated for the specific experiments, and the titers were determined by plaque assay on L2 cells.

**Treatment with IFN and 2-5A.** The cells were transfected with high-performance liquid chromatography (HPLC)-purified 10 μM 2-5A (p3A3) in 3 μg/ml Lipofectamine 2000 (Invitrogen) or Lipofectamine alone, and 4 h later, the cell lysates were harvested and RNA was isolated.

**IFNAR1-blocking-antibody treatment.** BMM cultures were treated with 0, 2, or 5 μg/ml of IFNAR1-blocking monoclonal antibody (MAb) (clone MAR1-5A3; BD Sciences) or an isotype control [purified NA/LE mouse IgG1(κ) clone107.3; BD Sciences] for 1 h at room temperature with gentle agitation before virus infection or mock infection (43).

**Bioassay for antiviral activity.** Supernatants recovered from cells that were infected with MHV strains at an MOI of 1 PFU/cell were exposed to 600 mJ · cm$^{-2}$ UVA light in a Stratalinker 1800 (Stratagene) to inactivate the virus. L2 mouse fibroblasts were treated with the UV-inactivated supernatants for 24 h and then infected with NDV-GFP at an MOI of 1 PFU/cell as described previously (35). Control cells were treated with 100 U/ml universal IFN-α (Quansys Biosciences, UT) for 24 h before NDV-GFP infection. At 12 and 24 h postinfection (hpi), cells were fixed in Dulbecco's phosphate-buffered saline (Gibco) containing 4% paraformaldehyde and examined for enhanced-GFP (EGFP) expression under an Eclipse TE2000-U fluorescence microscope (Nikon Instruments, Inc.). Images were acquired using NIS-Elements Basic Research microscope imaging software (Nikon Instruments, Inc.).

**IFN-β quantification.** IFN-β protein in supernatants of MHV-infected BMM was quantified with a commercial capture enzyme-linked immunosorbent assay (ELISA) kit (VeriKine Mouse Interferon Beta ELISA kit; PBL Laboratories, Piscataway, NJ) according to the manufacturer's instructions.

**rRNA degradation assay.** For quantification of rRNA cleavage, total RNA from virus-infected cells was isolated using an RNeasy kit (Qiagen) and quantified using a Nanodrop analyzer. Equal amounts of RNA were separated on RNA chips and analyzed with an Agilent 2100 Bioanalyzer (Agilent Technologies) as described previously (25, 44). RNA integrity numbers (referred to as RIN values) (45), a measurement of RNA integrity produced by the bioanalyzer, are also indicated.

**Immunoblotting.** Cells were treated with 0 or 100 units/ml of universal IFN-α for 4 h and then lysed in Nonidet P-40 (NP-40) buffer (1% NP-40, 2 mM EDTA, 10% glycerol, 150 mM NaCl, and 50 mM Tris, pH 8.0) containing protease inhibitors (Roche). Protein concentrations were measured using a DC protein assay kit (Bio-Rad). Supernatants were mixed 1:1 with 2× SDS-PAGE sample buffer. Samples were boiled, separated by SDS-10% PAGE, and transferred to polyvinylidene difluoride (PVDF) membranes. The blots were blocked with 5% nonfat milk and probed with the following antibodies directed against OAS1A (clone E-2; Santa Cruz; 1:200), OAS2 (clone G-9; Santa Cruz; 1:200), OAS3 (clone D-7; Santa Cruz; 1:200), mouse RNase L (goat polyclonal T-16; Santa Cruz; 1:200), mouse RNase L (rabbit polyclonal; 1:1,000) (46), and human RNase L (mouse monoclonal against human RNase L; 1:1,000) (11), as well as anti-GAPDH (glyceraldehyde-3-phosphate dehydrogenase)-horseradish peroxidase (HRP) (Abcam; 1:4,000), anti-β-tubulin–HRP (Abcam; 1:4,000). Goat anti-mouse IgG2a-HRP (Santa Cruz; 1:4,000), goat anti-mouse IgG-HRP (Santa Cruz; 1:5,000), donkey anti-goat IgG-HRP (Santa Cruz; 1:5,000), and donkey anti-rabbit IgG-HRP (GE Healthcare; 1:10,000) secondary antibodies were used to detect the primary antibodies of the appropriate species. The blots were visualized using Super Signal West Dura Extended Duration Substrate (Thermo Scientific). The blots were probed sequentially with antibodies directed against OAS1A, OAS2, OAS3, RNase L, and GAPDH, with blots being stripped between antibody treatments (see Fig. 4F and 5D). Parallel gels were run and blotted with individual antibodies (Fig. 2D and 3B). All immunoblots were performed at least twice.

**Quantifying IFNAR1 surface expression.** BMM and mixed glial cultures were stained with antibodies against GFAP (BD; clone 1B4), CD11b (eBioscience; clone M1/70), F4/80 (Biolegend; clone BM8), and the type I interferon receptor IFNAR1 (Biolegend; clone MAR1-5A3) or an isotype control (Biolegend; clone MOPC-21). Staining for GFAP was conducted following permeabilization with the Cytofix/Cytoperm Plus Fixation/Permeabilization kit (BD). Cells were analyzed with an LSR II (Becton Dickinson), and the resulting data were analyzed using FlowJo software (Treestar). Astrocytes (GFAP$^+$ CD11b$^-$ F4/80$^-$) and microglia (GFAP$^-$ CD11b$^+$ F4/80$^+$) from mixed cultures and macrophages (GFAP$^-$ CD11b$^+$ F4/80$^+$) from bone marrow-derived cultures were assessed for

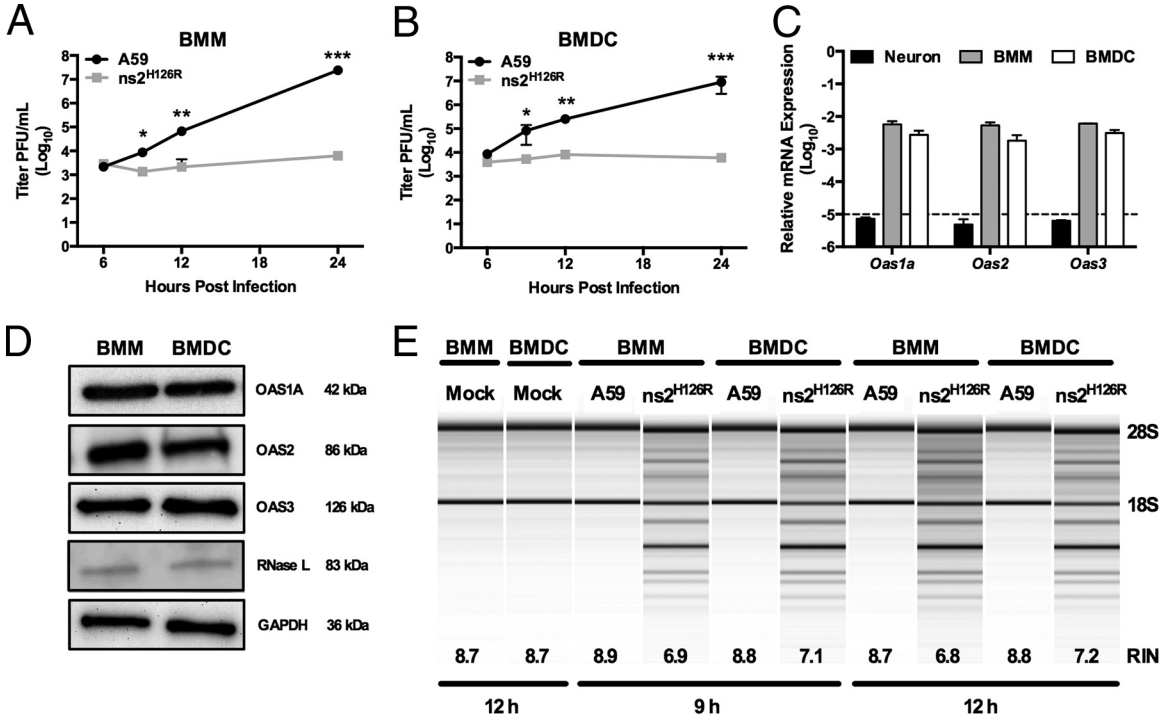


**FIG 2** Activation of RNase L by ns2$^{H126R}$ during infection of BMM and BMDC cultures. (A and B) BMM (A) and BMDC (B) cultures were infected with A59 or ns2$^{H126R}$ (1 PFU/cell), and at the times indicated, the virus titer was determined by plaque assay of the supernatant. The data are pooled from two independent experiments carried out in triplicate and are shown as means ± standard errors of the mean (SEM). *, $P < 0.05$; **, $P < 0.01$; ***, $P < 0.001$. (C) RNA was extracted from infected BMM, BMDC, and neuron cultures, and *Oas1a*, *Oas2*, and *Oas3* mRNA expression was quantified by qRT-PCR. mRNA expression levels relative to β-actin mRNA are expressed as $2^{-\Delta CT}$, where $\Delta C_T$ is equal to $C_{T\ \text{Target Gene}}$ minus $C_{T\ \beta\text{-actin}}$. The dashed line indicates the lower limit of detection. The data are from one representative experiment of two, each performed in triplicate. (D) Protein lysates from BMM and BMDC were electrophoresed in acrylamide gels and then probed with antibodies against OAS1A, OAS2, OAS3, RNase L (MAb), and GAPDH. (E) RNA was extracted from infected BMM and BMDC cultures at 9 and 12 h postinfection, as well as cultures 12 h post-mock infection, and rRNA degradation was assessed with a bioanalyzer. RIN values (45), a measurement of RNA integrity produced by the bioanalyzer, are also indicated. The positions of 28S and 18S rRNAs are indicated.

surface expression of IFNAR1 (Biolegend; clone MAR1-5A3) or an isotype control (Biolegend; clone MOPC-21).

Fluorescence intensity, dependent on both surface IFNAR1 density and cell surface area, was normalized by cell size using previously described methods (47). This allowed us to compare receptor densities between cells of different sizes. Briefly, forward scatter (FSC), a measure of cell volume, and side scatter (SSC), a measure of cell granularity, were used in a linear least-squares regression model to determine fluorescence intensities corrected for cell size and shape. Residuals from the model represent the variability in fluorescence that is not due to cell size and cell granularity. These residuals were offset by the sample-specific average fluorescence intensity to calculate the final values. Calculations and analysis were performed with MATLAB (Mathworks, Natick, MD).

**Statistical analysis.** Plotting of data and statistical analysis were performed using GraphPad Prism software (GraphPad Software, Inc., CA) Statistical significance was determined by an unpaired two-tailed Student *t* test.

## RESULTS

**Activation of RNase L during ns2$^{H126R}$ infection of dendritic cells correlates with high basal *Oas* gene expression.** We showed previously that while A59 antagonizes the OAS-RNase L pathway in myeloid lineage cells, including brain-resident microglia and liver-resident Kupffer cells, as well as BMM (2, 25, 29, 34), ns2$^{H126R}$, a mutant expressing an inactive PDE, failed to antagonize RNase L and consequently had severely restricted replication in these cell types. In contrast, replication of ns2$^{H126R}$ in primary cell types, including neurons, astrocytes, and hepatocytes, as well as in immortalized cell lines was as robust as that of A59 (2, 25, 29). We investigated whether other myeloid cells, such as dendritic cells, would behave similarly to macrophages upon infection. Thus, we compared the replication of A59 and ns2$^{H126R}$ in BMM and BMDC derived from B6 (WT) mice. As observed in BMM (Fig. 2A) (25, 29), BMDC (Fig. 2B) also restricted mutant-virus replication by 100-fold at 12 h ($P < 0.01$) and 1,000-fold after 24 h postinfection ($P < 0.001$).

We next compared the basal level of expression of *Oas* genes in BMDC with those of BMM and neurons. Using real-time quantitative RT-PCR, we quantified basal levels of expression of three *Oas* genes that encode catalytically active OAS proteins, *Oas1a*, *Oas2*, and *Oas3*, in WT BMM and WT BMDC cultures in comparison to primary neurons (Fig. 2C), which had been shown previously to express minimal basal levels of OAS genes and to be unable to restrict replication of ns2$^{H126R}$ (29). *Oas* mRNA expression levels in neurons, as expected, were under the limit of detection, and in comparison, basal mRNA expression levels of *Oas1a*, *Oas2*, and *Oas3* genes in WT BMM and WT BMDC were 1,000-fold greater than the minimal detectable level (Fig. 2C). Levels of OAS1A, OAS2, OAS3, and RNase L were similar in BMM and BMDC cultures, as assessed by immunoblotting (Fig. 2D). In order to compare RNase L activation during A59 and ns2$^{H126R}$ infection, we monitored the state of rRNA cleavage in WT BMM and

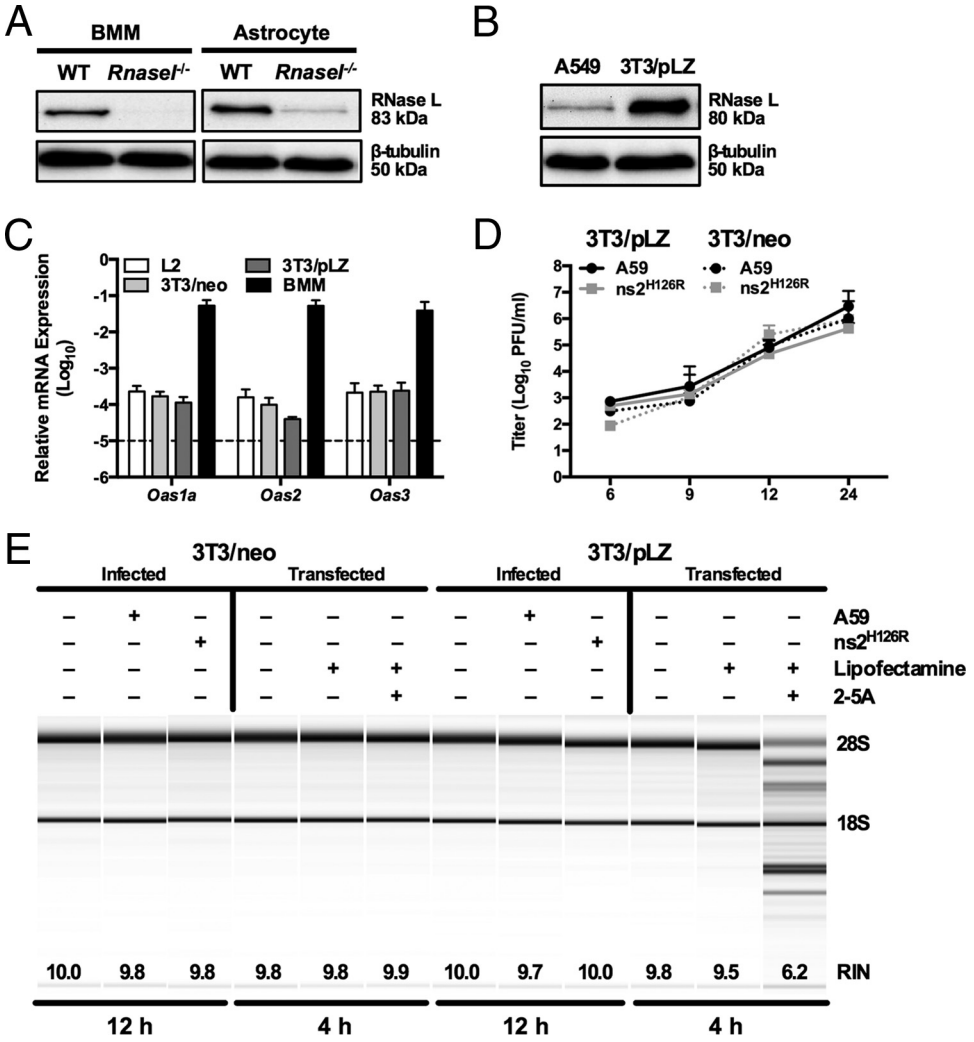


**FIG 3** Overexpression of RNase L is not sufficient to overcome low OAS levels to promote RNase L degradation. (A) Proteins were extracted from WT and *Rnasel*$^{-/-}$ BMM and astrocytes, electrophoresed in polyacrylamide gels, and probed by Western blotting with antibodies directed against RNase L (rabbit polyclonal) and β-tubulin. BMM and astrocyte lysates were electrophoresed on the same gel and blot; intervening lanes were removed and replaced by spaces between samples. (B) Proteins were extracted from human A549 and murine 3T3/pLZ cells, electrophoresed in polyacrylamide gels, and probed by Western blotting with antibodies directed against human RNase L and human β-tubulin. (C) RNA was extracted from L2, 3T3/pLZ, 3T3/neo, and BMM cultures, and basal expression levels of *Oas* mRNAs were quantified by qRT-PCR. mRNA expression levels relative to β-actin mRNA are expressed as $2^{-\Delta CT}$, where $\Delta C_T$ is equal to $C_{T\ \text{Target Gene}}$ minus $C_{T\ \beta\text{-actin}}$. The data are from one representative experiment of two (except for pLZ/neo mRNA), each performed in triplicate. The dashed line indicates the lower limit of detection. The error bars indicate SEM. (D) 3T3/pLZ and 3T3/neo cells were infected with A59 or ns2$^{H126R}$ (1 PFU/cell), and at the times indicated, the virus titer was determined by plaque assay of the supernatant. The data are pooled from two independent experiments (3T3/pLZ) or from one experiment (3T3/neo), each performed in triplicate. (E) 3T3/pLZ and 3T3/neo cells were mock infected or infected with A59 or ns2$^{H126R}$ (1 PFU/cell), and at 12 h postinfection, the cells were lysed and RNA was extracted. In a separate experiment, cells were transfected with 10 μM 2-5A in Lipofectamine or with Lipofectamine alone or were left untreated, and 4 h later, the cells were lysed and RNA was extracted. rRNA degradation was assessed with a bioanalyzer. 28S and 18S rRNAs are indicated.

BMDC infected with either ns2$^{H126R}$ or A59. The mutant virus ns2$^{H126R}$ induced rRNA cleavage at 9 and 12 h postinfection in BMM and BMDC (Fig. 2E). In contrast, A59 did not induce rRNA cleavage, similar to mock-infected cells, even at the later time points. As a more quantitative measurement, RIN values (45), a measurement of RNA integrity produced by the bioanalyzer, are also indicated. Thus, BMDC behaved similarly to BMM in activation of RNase L, and restriction of mutant virus and activation of RNase L correlated with elevated basal levels of OAS genes (29).

**Overexpression of RNase L does not overcome low basal *Oas* mRNA expression to promote RNase L activation by ns2$^{H126R}$.** We investigated whether the level of RNase L expression contributes to the differences observed between activation of RNase L and ns2$^{H126R}$ replication in myeloid and nonmyeloid cells. Thus, we compared BMM and astrocytes, the latter previously shown to express low levels of *Oas* genes compared with BMM (29). We quantified *Rnasel* protein levels by Western blotting in BMM and astrocytes using cells derived from *Rnasel*$^{-/-}$ mice as a negative control. RNase L protein expression levels were similar in BMM and astrocytes (Fig. 3A).

As RNase L activation is dependent on the production of 2-5A, we investigated whether overexpression of RNase L might enable

the low level of 2-5A produced by cells with low basal *Oas* mRNA expression to activate RNase L to degrade rRNA in response to ns2$^{H126R}$ infection. For this, we used a murine 3T3 cell line (3T3/pLZ) that stably overexpresses human RNase L from a cytomegalovirus (CMV) promoter at a level greater than 100-fold that of endogenous murine RNase L cells or endogenous human RNase L in A549 cells. Human RNase L was previously demonstrated to be activated in 3T3/pLZ cells when exposed to 2-5A (33). Indeed, RNase L protein levels are much greater in 3T3/pLZ cells than in A549 cells (Fig. 3B). (The A549 cell line is derived from human lung epithelium and expresses sufficient endogenous RNase L to be activated upon viral infection [48].) However, the 3T3/pLZ cells and control 3T3/neo cells lacking the human RNase L gene expressed a relatively low level of *Oas* mRNA, similar to that of the murine L2 cell line (29) (Fig. 3C). Upon infection of 3T3/pLZ cells with A59 and ns2$^{H126R}$, both viruses replicated to high titer, as in control 3T3/neo cells (Fig. 3D). RNase L was not activated by ns2$^{H126R}$, as assessed by rRNA degradation at 9 or 12 h postinfection (Fig. 3E). However, treatment of 3T3/pLZ cells, but not 3T3/neo cells, with 2-5A activated RNase L, demonstrating that human RNase L is indeed active in 3T3/pLZ cells. Thus, RNase L overexpression in 3T3/pLZ cells could not overcome the minimum 2-5A threshold needed to activate RNase L.

**RNase L is activated in the absence of virus-induced interferon in macrophages.** While A59 induces type I IFN expression in only a limited number of cell types, primarily myeloid cells (7, 49), the activation of RNase L during infection (with ns2$^{H126R}$) occurs only in the same limited cell types (7, 29, 49). Thus, we investigated whether virus-induced IFN was necessary to activate RNase L, presumably by further upregulating the already high basal levels of OAS expression. IFN production during MHV infection of macrophages is dependent on MDA5 signaling (7). Indeed, using a sensitive bioassay for antiviral activity (35), we confirmed that both A59- and ns2$^{H126R}$-infected WT BMM secreted detectable antiviral activity at 12 and 24 h postinfection (29), while infected MDA5-deficient (*Ifih1*$^{-/-}$) BMM failed to secrete detectable levels (Fig. 4A). We confirmed the presence of IFN in these WT BMM supernatants by quantifying the level of IFN-β secreted at 12 h postinfection by ELISA. In WT BMM, MHV infection elicited detectable but low levels (20 to 25 pg/ml) of IFN-β (Fig. 4B), while *Ifih1*$^{-/-}$ BMM cultures did not produce detectable IFN-β. Replication of ns2$^{H126R}$ was 100-fold reduced at 12 hpi and 1,000-fold attenuated after 24 h in *Ifih1*$^{-/-}$ macrophages (Fig. 4D) compared to A59 in WT BMM (Fig. 4C) (25), indicating that ns2$^{H126R}$ replication is restricted in BMM even in the absence of virus-induced IFN production.

Consistent with the above-mentioned findings, we observed similar levels of *Oas* and *Rnasel* mRNAs in WT and *Ifih1*$^{-/-}$ BMM (Fig. 4E). In addition, the corresponding protein levels of OAS1A, OAS2, OAS3, and RNase L appeared to be at least as high in *Ifih1*$^{-/-}$ BMM as in WT BMM (Fig. 4F). While these immunoblot data show a small to modest increase in OAS1A, OAS2, OAS3, and RNase L levels in *Ifih1*$^{-/-}$ cells compared to the WT, other replicates failed to show any detectable differences (data not shown). Furthermore, we compared the levels of other ISGs in WT and *Ifih1*$^{-/-}$ BMM and found little difference in their relative mRNA expression levels, with the exception of MDA5, which, as expected, was not expressed in *Ifih1*$^{-/-}$ BMM cultures (Fig. 4G). Finally, RNase L activation was observed in both genotypes of BMM by 12 h postinfection with ns2$^{H126R}$, while it was also evident at 9 h in WT cells. Thus, infection with ns2$^{H126R}$ activated RNase L in the absence of virus-induced IFN (Fig. 4H).

**Basal interferon signaling is required for maintenance of adequate *Oas* mRNA levels and RNase L activation in macrophages.** Basal IFN signaling is necessary to maintain basal expression of ISGs, which enables the cell to quickly respond to infection by inducing IFN, as well as upregulating antiviral ISGs (50). Indeed, we have reported much higher levels of ISG expression in myeloid cells that are able to induce IFN and activate RNase L during MHV infection than in other cell types (2, 29). As in the data shown in Fig. 4C, ns2$^{H126R}$ was preferentially restricted compared to A59 in WT BMM starting at 9 h and 100 to 1,000-fold decreased from 12 to 24 h after infection (Fig. 5A). However, replication of ns2$^{H126R}$ was fully recovered in *Ifnar1*$^{-/-}$ BMM (Fig. 5B).

We compared the expression of several *Oas* genes in WT and *Ifnar1*$^{-/-}$ BMM and found reduced expression of *Oas1a* ($P < 0.01$), *Oas2* ($P < 0.001$), and *Oas3* ($P < 0.01$) mRNAs in *Ifnar1*$^{-/-}$ BMM, presumably due to loss of basal IFN signaling, but no significant difference in *Rnasel* mRNA expression (Fig. 5C). Furthermore, we compared the basal protein expression levels of OAS1A, OAS2, and RNase L in BMM derived from WT or *Ifnar1*$^{-/-}$ mice. OAS1A, OAS2, and OAS3 proteins were undetectable in cell lysates from *Ifnar1*$^{-/-}$ BMM cultures (Fig. 5D) with or without prior IFN treatment. While OAS proteins are modestly induced by IFN treatment of WT BMM, RNase L protein expression is not dependent on IFNAR expression, nor is it induced by IFN treatment. Basal expression levels of other ISG mRNAs (including *Ifih1* [$P < 0.05$]; *Ddx58* [$P < 0.01$]; and *Ifit1*, *Ifit2*, *Isg15*, and *Irf7* [$P < 0.0001$]) were significantly decreased in the absence of IFNAR1 signaling compared to WT BMM (Fig. 5E). The *Irf3* expression levels, which are independent of IFNAR1 signaling (51), were similar in WT and *Ifnar1*$^{-/-}$ BMM. Moreover, *Ifnb* expression levels were comparable in both genotypes and near the limit of detection (Fig. 5E). Additionally, degradation of rRNA was assessed in lysates from infected BMM cultures at 9 and 12 h postinfection. In WT BMM cultures, ns2$^{H126R}$ infection induced rRNA degradation; however, in *Ifnar1*$^{-/-}$ BMM cultures, RNase L was not activated and rRNA degradation was not observed (Fig. 5F), supporting the notion that adequate basal levels of OAS gene expression are required for activation of RNase L upon virus infection.

We hypothesized that the difference in basal ISG expression between macrophages and astrocytes could be at least in part due to the cell surface expression level of the type I interferon receptor, IFNAR1. Cells with higher IFNAR1 surface expression might promote higher basal IFN signaling and ISG levels and therefore be more likely to activate RNase L in the presence of dsRNA early during ns2$^{H126R}$ infection. To assess surface IFNAR1 expression on BMM, microglia, and astrocytes, BMM and primary astrocyte/microglia cultures were stained for identifying markers and IFNAR1 and then analyzed by flow cytometry. As astrocytes displayed a larger range in size than macrophages (data not shown), we applied a size normalization algorithm to determine the density of surface IFNAR1. Using previously described methods (47), fluorescence intensity, dependent on both surface IFNAR1 density and cell surface area, was normalized by cell size to enable comparison of the extents of relative IFNAR1 expression across cell types. The surface density of IFNAR1 was higher in microglia and BMM than in astrocytes (Fig. 5G), perhaps contributing to the greater extent of basal ISGs detected in myeloid cells.

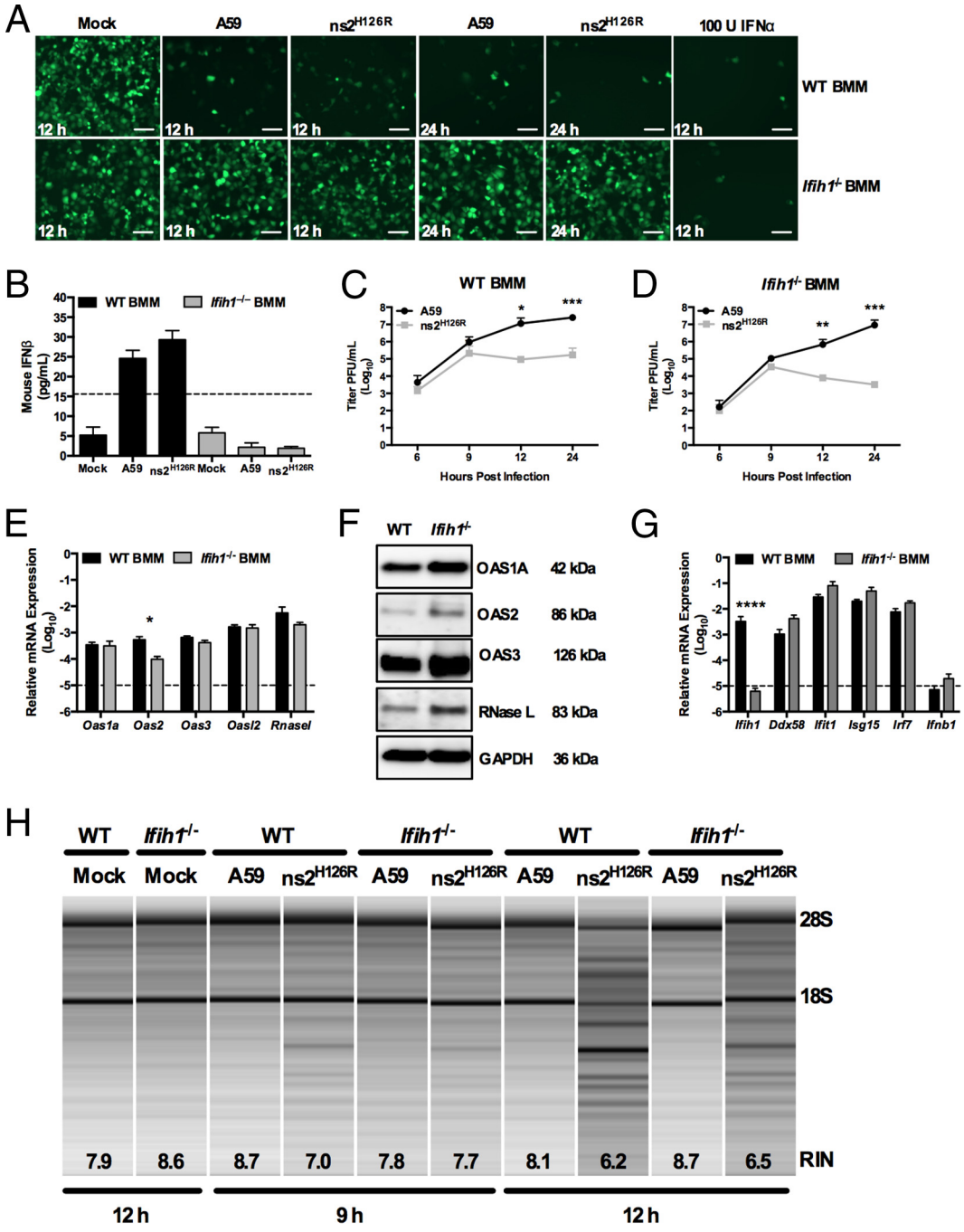


**FIG 4** Infection of *Ifih1*$^{-/-}$ macrophages with A59 and ns2$^{H126R}$. (A) WT or *Ifih1*$^{-/-}$ BMM cultures were either mock infected or infected with A59 or ns2$^{H126R}$ (1 PFU/cell). At 12 h postinfection, the supernatants were treated with UV light to inactivate the virus and incubated with L2 mouse fibroblasts for 24 h, followed by infection with NDV-GFP (1 PFU/cell). As a positive control, L2 cells were treated with IFN-α for 24 h and then infected with NDV-GFP. At 12 or 24 h postinfection, the cells were fixed and examined for EGFP expression by microscopy. The scale bars represent 50 μm. (B) Supernatants taken at 12 h postinfection from the same mock-infected or A59- and ns2$^{H126R}$-infected WT and *Ifih1*$^{-/-}$ BMM cultures were analyzed by ELISA for mouse IFN-β with a VeriKine kit. The limit of detection is indicated by the dashed line. The data are from one representative experiment of two. (C and D) WT BMM (C) and *Ifih1*$^{-/-}$ BMM (D) cultures were infected with A59 and ns2$^{H126R}$ (1 PFU/cell), and at the times indicated, the virus titer was determined by plaque assay of the supernatant. The data are pooled from two independent experiments performed in triplicate and are shown as means ± SEM. *, $P < 0.05$; **, $P < 0.01$; ***, $P < 0.001$. (E and G) mRNA expression levels relative to β-actin mRNA are expressed as $2^{-\Delta CT}$, where $\Delta C_T$ is equal to $C_{T\,\text{Target Gene}}$ minus $C_{T\,\beta\text{-actin}}$. The dashed lines indicate the lower limit of detection. The data shown are pooled from two independent experiments, each performed in triplicate, and are shown as means and SEM. *, $P < 0.05$; ****, $P < 0.0001$. (F) Proteins were extracted from WT and *Ifih1*$^{-/-}$ BMM and probed by Western blotting with antibodies directed against OAS1A, OAS2, OAS3, RNase L (MAb), and GAPDH. (H) RNA was extracted from infected WT and *Ifih1*$^{-/-}$ BMM cultures at 9 and 12 h postinfection, as well as cultures 12 h post-mock infection, and rRNA degradation was assessed with a bioanalyzer. 28S and 18S rRNAs are indicated.

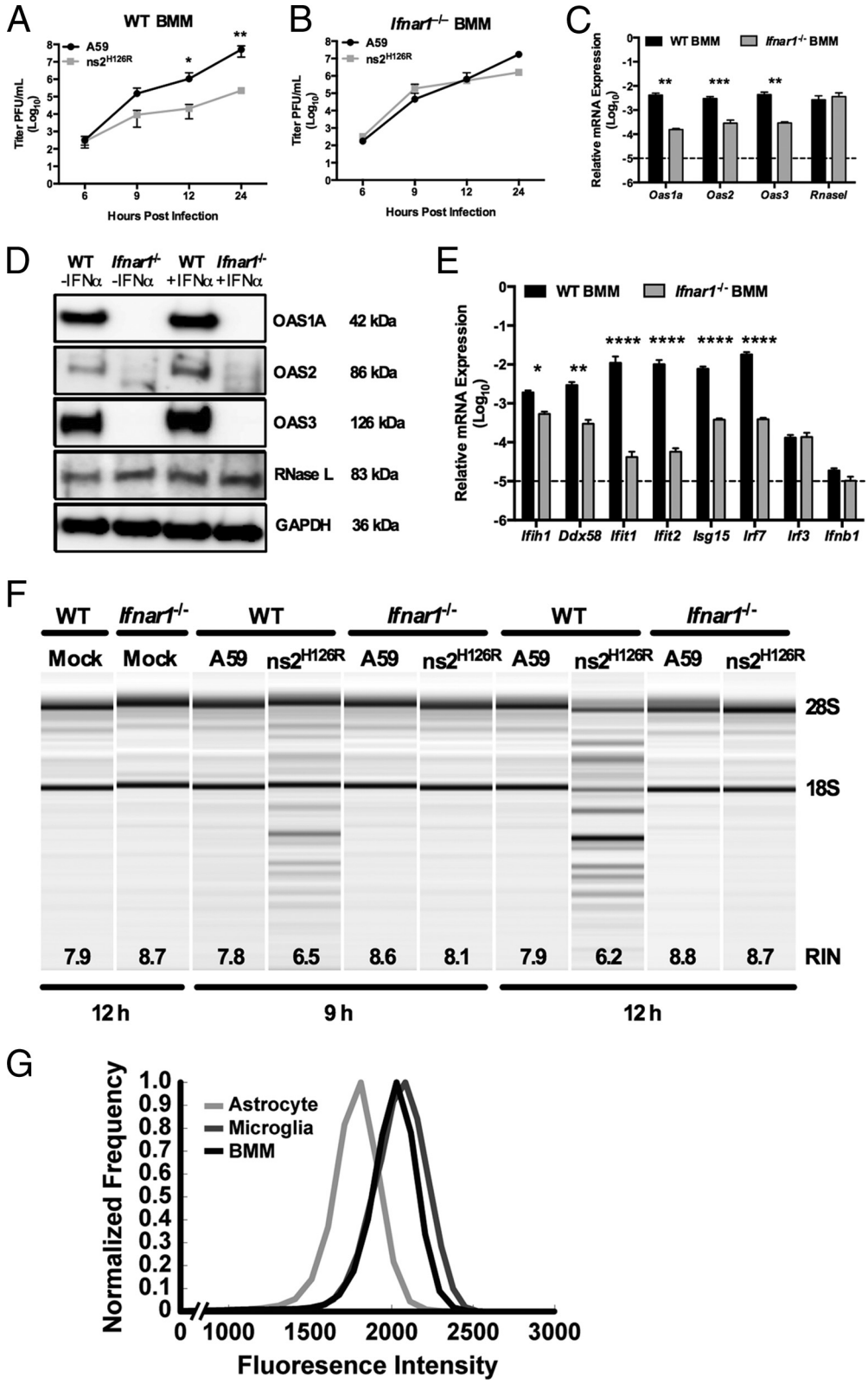


**FIG 5** RNase L is not activated during infection of *Ifnar1*$^{-/-}$ macrophages. (A and B) WT (A) and *Ifnar1*$^{-/-}$ (B) BMM cultures were infected with A59 or ns2$^{H126R}$ (1 PFU/cell), and at the times indicated, the virus titer was determined by plaque assay of the supernatant. The data are pooled from two independent experiments performed in triplicate and are shown as means ± SEM. *, $P < 0.05$; **, $P < 0.01$. (C) RNA was extracted from uninfected WT and *Ifnar1*$^{-/-}$ BMM cultures, and *Oas1a*, *Oas2*, *Oas3*, and *Rnasel* mRNAs were quantified by qRT-PCR. mRNA expression levels relative to β-actin mRNA are expressed as $2^{-\Delta CT}$, where $\Delta C_T$ is equal to $C_{T\ \text{Target Gene}}$ minus $C_{T\ \beta\text{-actin}}$. The dashed line indicates the lower limit of detection. The data are pooled from two independent experiments, each performed in triplicate, and are shown as means and SEM. **, $P < 0.01$; ***, $P < 0.001$. (D) WT and *Ifnar1*$^{-/-}$ BMM cultures were either mock

**Modulation of surface IFNAR1 activity regulates basal *Oas* mRNA expression and RNase L activation.** To complement the infections in *Ifnar1*$^{-/-}$ BMM and to further explore the relationship between IFN signaling, basal *Oas* gene expression, and activation of RNase L, we aimed to modulate IFNAR1 activity on WT BMM so that adequate basal IFN signaling would be maintained but the cells would not be capable of further upregulating ISGs upon infection. We used a monoclonal antibody (MAR1-5A3) specific for the IFNAR1 subunit of the murine IFN receptor that binds to cell surface IFNAR1 and blocks ligand-induced intracellular receptor signaling and induction of ISGs (37, 52–54). Following 1 h of 2-μg/ml antibody pretreatment of WT BMM, there was no increase in *Oas1*, *Oas2*, or *Oas3* mRNA expression following infection, and the basal levels of mRNAs in mock-infected cells were the same as in no-MAb controls (Fig. 6A to C). Other ISGs, for example, *Ifit1*, also failed to be induced following infection (data not shown). Under these conditions, RNase L activity was still activated by infection with ns2$^{H126R}$ at 9 and 12 h postinfection (Fig. 6G), resulting in restriction of viral replication (Fig. 6E). Thus, with a 1-h pretreatment with 2 μg/ml of antibody, basal mRNA levels of OAS genes are maintained and BMM retain the ability to restrict MHV and activate RNase L in the absence of upregulation of *Oas* expression levels. However, the use of a higher dose of antibody (5 μg/ml) recapitulated the phenotype observed in *Ifnar1*$^{-/-}$ BMM in that basal levels of *Oas* mRNA expression in mock-infected mice were decreased approximately 10-fold (Fig. 6A to C, compare mock-infected, 5 μg/ml MAb-treated to mock-infected, no MAb treatment). In addition, *Oas* mRNA levels were not induced by infection and activation of RNase L did not occur, as assessed by an rRNA degradation assay (Fig. 6G), and replication of ns2$^{H126R}$ was no longer restricted (Fig. 6F). It is important to note that treatment of cells with an isotype control antibody had no effect on replication of A59 or ns2$^{H126R}$ and that the replication of ns2$^{H126R}$ was restricted following treatment with isotype control antibody (Fig. 6F), indicating the effects were specific for IFNAR1 (Fig. 6E and F). Thus, consistent with our observations from infection of *Ifnar1*$^{-/-}$ and *Ifih1*$^{-/-}$ BMM (Fig. 4 and 5), activation of RNase L correlated with an *Oas* gene basal level of expression and did not require further upregulation during infection.

## DISCUSSION

OAS and RNase L comprise a potent antiviral pathway that is activated during viral infection (13). The dsRNA generated during viral infection is sensed by several OAS proteins that respond by synthesizing 2-5A, which in turn induces the dimerization and activation of RNase L. RNase L activation reduces viral replication and spread by degrading host and viral RNA-limiting protein synthesis and eventually leading to apoptosis (14). While the current paradigm is that upregulation of OAS transcription by type I interferon during virus infection is needed to provide enough OAS protein to activate the pathway, our data indicate that BMM are prearmed with high basal levels of OAS, sufficient to allow activation of RNase L upon sensing dsRNA early in infection. In addition to BMM, brain-resident microglia (29), liver-resident Kupffer cells (data not shown), and BMDC (Fig. 2) show high basal levels of OAS gene expression. Thus, in myeloid cells, RNase L activation (Fig. 1, right) is not dependent on virus induction of IFN (Fig. 1, left). This is especially important when considering a virus like MHV that induces IFN only late in infection (49). Conversely, in many nonmyeloid cell types, including primary hepatocytes, neurons, astrocytes, and murine cell lines, *Oas* expression levels are significantly lower. In these cells, ns2$^{H126R}$ infection fails to induce RNase L and MHV replicates to high titer, independent of ns2 PDE activity. These data suggest that myeloid cells are able to quickly respond to early virus infection before IFN is induced, thereby sparing nonrenewable neighboring parenchymal cells from infection.

The correlation of RNase L activation with high basal *Oas* gene expression suggests that production of 2-5A is the limiting step in activation. While *Oas* expression levels were quite variable among murine cell types, we found similar levels of RNase L expression in murine BMM and astrocytes (Fig. 3A), cell types expressing high and low levels of *Oas* genes, respectively. Furthermore, basal levels of *RNasel* transcripts and proteins were not dependent on IFNAR signaling in BMM (Fig. 5C and D). However, to investigate whether a high level of RNase L could overcome the requirement for high OAS levels to produce 2-5A, we carried out infections in murine 3T3/pLZ cells, which overexpress RNase L to a level about 100-fold greater than that of endogenous RNase L (33). Since MHV induces type I IFN in myeloid cells only and not mouse fibroblast lines, RNase L activation depends on basal OAS expression levels, and RNase L was not activated in this cell type by either A59 or ns2$^{H126R}$, while treatment with 2-5A directly activated RNase L and promoted RNA degradation in 3T3/pLZ but not 3T3/neo cells (Fig. 3E). These findings indicate that OAS activity is the limiting step for RNase L activation during infection, as extremely high levels of RNase L were not sufficient to overcome insufficient levels of *Oas* gene expression.

We present further evidence that in myeloid cells, RNase L can be activated in the absence of MDA5, the recognition receptor necessary for the induction of IFN during MHV infection (7), as long as *Oas* gene expression remains at an adequate level. However, we did observe delays in both RNase L activation and restriction of ns2$^{H126R}$ replication in *Ifih1*$^{-/-}$ compared with B6 BMM (Fig. 4C, D, and H, compare 9- and 12-h time points), suggesting that the induction of IFN during infection in B6 BMM may accelerate the activation of RNase L. The reduced levels of *Oas* gene

treated or treated with 100 U/ml of universal IFN-α for 4 h; protein was extracted, electrophoresed in polyacrylamide gels, and probed with antibodies directed against OAS1A, OAS2, OAS3, RNase L (MAb), and GAPDH. (E) RNA was extracted from uninfected WT and *Ifnar1*$^{-/-}$ BMM cultures, and ISG mRNAs were quantified by qRT-PCR. mRNA expression levels relative to β-actin mRNA are expressed as $2^{-\Delta CT}$, where $\Delta C_T$ is equal to $C_{T\ \text{Target Gene}}$ minus $C_{T\ \beta\text{-actin}}$. The dashed line indicates the lower limit of detection. The data are pooled from three independent experiments, each performed in triplicate, and are shown as means and SEM. *, $P < 0.05$; **, $P < 0.01$; ****, $P < 0.0001$. (F) RNA was extracted from BMM cultures at 9 and 12 h postinfection, as well as from cultures 12 h post-mock infection, and rRNA degradation was assessed with a bioanalyzer. 28S and 18S rRNAs are indicated. (G) Astrocytes and microglia from mixed glial cultures and macrophages from bone marrow-derived cultures were stained with cell-type-specific antibodies, as well as for IFNAR1, and analyzed by flow cytometry with an LSR II (Becton Dickinson), and the resulting data were analyzed using FlowJo software (Treestar). Astrocytes (GFAP$^+$ CD11b$^-$ F4/80$^-$), microglia (GFAP$^-$ CD11b$^+$ F4/80$^+$), and macrophages (GFAP$^-$ CD11b$^+$ F4/80$^+$) were assessed for surface expression of IFNAR1. The data are from one representative experiment of two, each performed with triplicate cultures of each cell type.

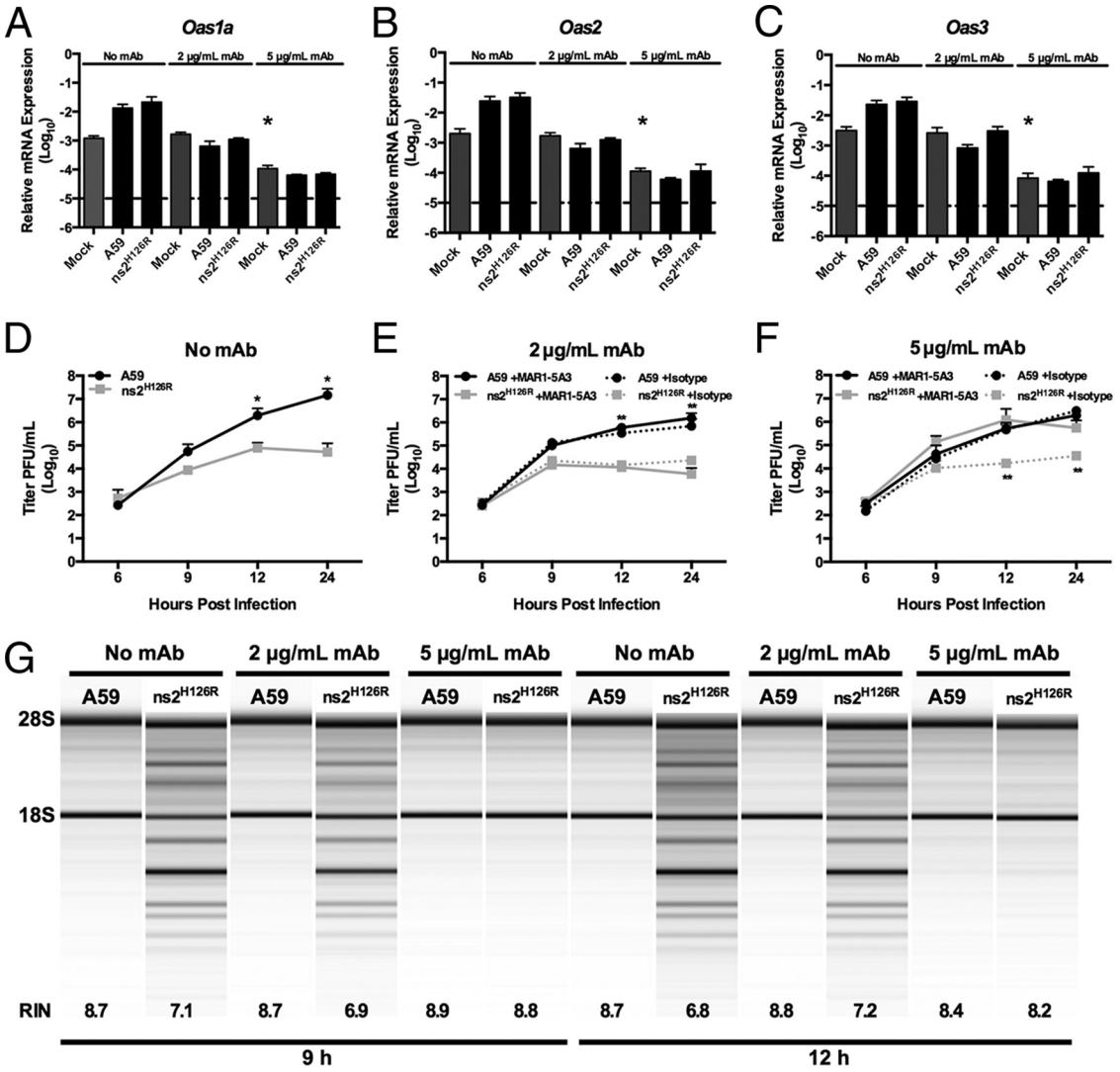


**FIG 6** Activation of RNase L activity in BMM treated with IFNAR1-blocking MAR1-5A3 MAb. WT BMM were treated with 2 μg/ml or 5 μg/ml MAR1-5A3 IFNAR1-blocking MAb or no MAb or with isotype control Ab (panels E and F only) for 1 h before infection with A59 or ns2$^{H126R}$ (1 PFU/cell) or mock infection. RNA was extracted from the cells at time zero post-mock infection and 12 h post-virus infection. (A to C) Expression levels of *Oas1a* (A), *Oas2* (B), and *Oas3* (C) mRNAs were quantified by qRT-PCR. The levels of mRNA expression relative to β-actin mRNA are expressed as $2^{-\Delta CT}$, where $\Delta C_T$ is equal to $C_{T\,\text{Target Gene}}$ minus $C_{T\,\beta\text{-actin}}$. The dashed lines indicate the lower limit of detection. The data are pooled from two independent experiments, each performed in triplicate, and are shown as means and SEM. The values for mock-infected, 5 μg/ml MAb-treated cells are significantly different from those for mock-infected, 0 MAb- or 2 μg/ml MAb-treated cells, *, $P < 0.05$. (D to F) Virus titers of supernatants from A59- or ns2$^{H126R}$-infected BMM cultures pretreated with no MAb (D), 2 μg/ml IFNAR1-blocking MAb (solid lines) or istoype control Ab (dotted lines) (E), and 5 μg/ml of IFNAR1 blocking MAb (solid lines) or isotype control Ab (dotted lines) (F) were determined by plaque assay. The data are pooled from three independent experiments (except for isotype control-treated cells, which were assayed one time), each performed in triplicate, and are shown as means and SEM. *, $P < 0.05$; **, $P < 0.01$. (G) RNA was extracted at 9 and 12 h postinfection from BMM cultures that had been pretreated with MAb as indicated, and rRNA degradation was assessed with a bioanalyzer. 28S and 18S rRNAs are indicated. RNA from mock-infected cultures appeared similar to that from A59-infected cells (not shown), as in Fig. 2E, 3E, 4H, and 5F.

expression in BMM derived from *Ifnar1*$^{-/-}$ mice or B6 mice treated with 5 μg/ml IFNAR1-blocking antibody preclude the activation of RNase L during ns2$^{H126R}$ infection. These data suggest that the basal level of *Oas* expressed in BMM derived from WT B6 or *Ifih1*$^{-/-}$ mice is both necessary and adequate to produce enough 2-5A to activate RNase L in the absence of virus-induced IFN.

IFN is vital for control of early MHV infection *in vivo* (6–8). However, MHV and other coronaviruses, such as severe acute respiratory syndrome coronavirus (SARS-CoV) and Middle East respiratory syndrome coronavirus (MERS-CoV), are poor inducers of IFN, as they actively avoid and/or inhibit a robust type I IFN response in infected cells (49, 55–60). In the case of MHV, IFN is not detected during infection of cell lines nor in several types of primary cells *in vitro*, including the main types of cells infected in the major targets of infection, the brain (neurons, astrocytes, and oligodendrocytes) and the liver (hepatocytes). However, MHV does induce IFN in macrophages and microglia in the brain (7), as well as pDCs *in vivo* (17), and in myeloid cells *in vitro* (7). These are the same types of cells that express high levels of basal *Oas* genes and that activate RNase L in response to ns2$^{H126R}$, probably as a consequence of the high expression levels of ISGs, including

MDA5 and the transcription factors necessary for IFN induction (2, 29). Thus, *in vivo*, low-*Oas*-gene-expressing cells may be induced by paracrine IFN to increase OAS levels, enabling viral activation of RNase L. Indeed, in previous experiments reported by our laboratory, pretreatment of astrocytes or neurons with IFN did increase the levels of *Oas* gene expression (29). However, IFN pretreatment also resulted in decreased titers of both A59 and ns2$^{H126R}$, and the absence of activation of RNase L in those experiments was suggested to be a consequence of reduced ability of both A59 and ns2$^{H126R}$ to replicate and produce dsRNA following IFN pretreatment (29). We infer from these data that, not surprisingly, IFN treatment induces many antiviral ISGs, some of which inhibit viral replication without the activation of RNase L. Furthermore, high basal *Oas* levels are necessary for the activation of RNase L by MHV lacking a functional viral PDE.

Type I IFNs are produced constitutively in very small quantities, barely detectable at the mRNA and protein levels in some cell types, such as BMM cultures (Fig. 5E and data not shown) and undetectable in most other cell types we have tested (data not shown). However, this low level of constitutive IFN is believed to have many important effects for the host, including cytokine induction, immune cell activity, maintenance and mobilization of hematopoietic stem cells, and antitumor effects (50, 61). In addition, and most relevant to this work, constitutive IFN signaling is important for maintaining adequate basal levels of ISGs to promote rapid and efficient responses to microbial invasion, as evidenced by the extreme sensitivity of *Ifnar1*$^{-/-}$ mice to many viruses, including MHV. It is important that the levels of constitutive IFN be carefully regulated, as excessive IFN can have pathological effects, contributing to several autoimmune diseases and promoting cancer (50, 61, 62).

Little is known about the regulation of secretion or activity of constitutive IFN. While the transcriptional regulation of IFN-β following viral infection has been extensively characterized, less is known regarding the transcriptional regulation of constitutive basal IFN-β expression. However, it is known that constitutive IFN production is dependent on IRF-3 and IRF-7, two major transcription factors driving type I IFN transcription following viral infection (51, 63), but repressed by IRF-2, which binds to the IFN-β promoter and contributes to tight control of basal expression (64, 65). We found that astrocytes have a significantly higher basal *Irf2* mRNA expression level than BMM (data not shown).

There is some evidence that the IFNAR1 expression level may play a role in viral pathogenesis, as it was recently reported that the encephalitic flaviviruses tick-borne encephalitis virus and West Nile virus antagonize IFN signaling by downregulating IFNAR1 surface expression, thus reducing IFN-β-stimulated antiviral gene induction and compromising host control of infection (66). Interestingly, in a reovirus model of myocarditis, surface expression levels of IFNAR, as well as basal ISG levels, were higher in cardiac fibroblasts than in cardiac myocytes. It was suggested that upon exposure to IFN, cardiac fibroblasts could quickly develop an antiviral state and thereby avoid serving as a site of replication and spread to the nonrenewable cardiac myocytes (67). Similarly, our data suggest that astrocytes have relatively low IFNAR1 surface expression compared to microglia in the brain or BMM (Fig. 5G), which could contribute to the lower level of basal ISG expression. We found that astrocytes and neurons did not activate RNase L activity in response to a variety of viruses, including MHV, encephalomyocarditis virus, Sendai virus, and LaCrosse virus (29), likely a consequence of low basal ISG expression. Terminally differentiated astrocytes and neurons might have limited IFN responsiveness and secretion to prevent damage to the CNS. This is in contrast to renewable myeloid cells, such as macrophages and microglia, that are primed to respond to viral infection and reduce viral spread to other cell types.

As described above, we have found that activation of RNase L correlates with high basal *Oas* mRNA expression in analysis of myeloid versus nonmyeloid cell types, in B6 versus *Ifih1*$^{-/-}$ and Ifnar1$^{-/-}$ BMM, and in cells treated with antibody to IFNAR1 versus untreated controls. Basal expression of OAS1a, OAS2, and OAS3 proteins was dependent on IFNAR expression, and levels in myeloid cells were sufficient to activate RNase L upon viral infection. There are few, if any, data indicating which *Oas* genes are most important for RNase L activation in response to viral infections. Work is being conducted to determine the roles of individual *Oas* genes in activating RNase L.

## ACKNOWLEDGMENTS

This work was supported by NIH grants R01-NS081008 and R01-NS054695 (S.R.W.), R01-AI104887 (S.R.W. and R.H.S.), and R01-CA044059 (R.H.S.). L.D.B. and K.M.R. were each supported in part by training grant T32-AI007324, and Z.B.Z. was supported in part by T32-NS-007180.

We are grateful to Babal Jha (Cleveland Clinic) for the HPLC-purified 2-5A.

## FUNDING INFORMATION

HHS | NIH | National Cancer Institute (NCI) provided funding to Robert H. Silverman under grant number R01-CA044059. HHS | NIH | National Institute of Allergy and Infectious Diseases (NIAID) provided funding to L. Dillon Birdwell, Yize Li, Ruth Elliott, Kristine M. Rose, Robert H. Silverman, and Susan R. Weiss under grant numbers R01-AI104887 and T32-AI007324. HHS | NIH | National Institute of Neurological Disorders and Stroke (NINDS) provided funding to L. Dillon Birdwell, Zachary Bestor Zalinger, Yize Li, Ruth Elliott, Kristine M. Rose, and Susan R. Weiss under grant numbers R01-NS081008, R01-NS054695, and T32-NS-007180.

The funders had no role in study design, data collection and interpretation, or the decision to submit the work for publication.

## REFERENCES

1. **Navas-Martin S, Weiss SR.** 2003. SARS: lessons learned from other coronaviruses. Viral Immunol **16:**461–474. http://dx.doi.org/10.1089/088282403771926292.
2. **Zhao L, Rose KM, Elliott R, Van Rooijen N, Weiss SR.** 2011. Cell-type-specific type I interferon antagonism influences organ tropism of murine coronavirus. J Virol **85:**10058–10068. http://dx.doi.org/10.1128/JVI.05075-11.
3. **Lavi E, Gilden DH, Wroblewska Z, Rorke LB, Weiss SR.** 1984. Experimental demyelination produced by the A59 strain of mouse hepatitis virus. Neurology **34:**597–603. http://dx.doi.org/10.1212/WNL.34.5.597.
4. **Marten NW, Stohlman SA, Atkinson RD, Hinton DR, Fleming JO, Bergmann CC.** 2000. Contributions of CD8+ T cells and viral spread to demyelinating disease. J Immunol **164:**4080–4088. http://dx.doi.org/10.4049/jimmunol.164.8.4080.
5. **Marten NW, Stohlman SA, Bergmann CC.** 2001. MHV infection of the CNS: mechanisms of immune-mediated control. Viral Immunol **14:**1–18. http://dx.doi.org/10.1089/08828240151061329.
6. **Ireland DD, Stohlman SA, Hinton DR, Atkinson R, Bergmann CC.** 2008. Type I interferons are essential in controlling neurotropic coronavirus infection irrespective of functional CD8 T cells. J Virol **82:**300–310. http://dx.doi.org/10.1128/JVI.01794-07.
7. **Roth-Cross JK, Bender SJ, Weiss SR.** 2008. Murine coronavirus mouse

hepatitis virus is recognized by MDA5 and induces type I interferon in brain macrophages/microglia. J Virol **82:**9829–9838. http://dx.doi.org/10.1128/JVI.01199-08.

8. **Cervantes-Barragan L, Zust R, Weber F, Spiegel M, Lang KS, Akira S, Thiel V, Ludewig B.** 2007. Control of coronavirus infection through plasmacytoid dendritic-cell-derived type I interferon. Blood **109:**1131–1137.
9. **Kumagai Y, Takeuchi O, Akira S.** 2008. Pathogen recognition by innate receptors. J Infect Chemother **14:**86–92. http://dx.doi.org/10.1007/s10156-008-0596-1.
10. **Takeuchi O, Akira S.** 2007. Recognition of viruses by innate immunity. Immunol Rev **220:**214–224. http://dx.doi.org/10.1111/j.1600-065X.2007.00562.x.
11. **Dong B, Silverman RH.** 1995. 2-5A-dependent RNase molecules dimerize during activation by 2-5A. J Biol Chem **270:**4133–4137. http://dx.doi.org/10.1074/jbc.270.8.4133.
12. **Malathi K, Dong B, Gale M, Jr, Silverman RH.** 2007. Small self-RNA generated by RNase L amplifies antiviral innate immunity. Nature **448:**816–819. http://dx.doi.org/10.1038/nature06042.
13. **Silverman RH.** 2007. Viral encounters with 2′,5′-oligoadenylate synthetase and RNase L during the interferon antiviral response. J Virol **81:**12720–12729. http://dx.doi.org/10.1128/JVI.01471-07.
14. **Zhou A, Paranjape J, Brown TL, Nie H, Naik S, Dong B, Chang A, Trapp B, Fairchild R, Colmenares C, Silverman RH.** 1997. Interferon action and apoptosis are defective in mice devoid of 2′,5′-oligoadenylate-dependent RNase L EMBO J **16:**6355–6363.
15. **Durbin JE, Fernandez-Sesma A, Lee CK, Rao TD, Frey AB, Moran TM, Vukmanovic S, Garcia-Sastre A, Levy DE.** 2000. Type I IFN modulates innate and specific antiviral immunity. J Immunol **164:**4220–4228. http://dx.doi.org/10.4049/jimmunol.164.8.4220.
16. **Muller U, Steinhoff U, Reis LF, Hemmi S, Pavlovic J, Zinkernagel RM, Aguet M.** 1994. Functional role of type I and type II interferons in antiviral defense. Science **264:**1918–1921. http://dx.doi.org/10.1126/science.8009221.
17. **Cervantes-Barragan L, Lewis KL, Firner S, Thiel V, Hugues S, Reith W, Ludewig B, Reizis B.** 2012. Plasmacytoid dendritic cells control T-cell response to chronic viral infection. Proc Natl Acad Sci U S A **109:**3012–3017. http://dx.doi.org/10.1073/pnas.1117359109.
18. **Silverman RH.** 2007. A scientific journey through the 2-5A/RNase L system. Cytokine Growth Factor Rev **18:**381–388. http://dx.doi.org/10.1016/j.cytogfr.2007.06.012.
19. **Kakuta S, Shibata S, Iwakura Y.** 2002. Genomic structure of the mouse 2′,5′-oligoadenylate synthetase gene family. J Interferon Cytokine Res **22:**981–993. http://dx.doi.org/10.1089/10799900260286696.
20. **Mashimo T, Glaser P, Lucas M, Simon-Chazottes D, Ceccaldi PE, Montagutelli X, Despres P, Guenet JL.** 2003. Structural and functional genomics and evolutionary relationships in the cluster of genes encoding murine 2′,5′-oligoadenylate synthetases. Genomics **82:**537–552. http://dx.doi.org/10.1016/S0888-7543(03)00176-9.
21. **Silverman RH, Weiss SR.** 2014. Viral phosphodiesterases that antagonize double-stranded RNA signaling to RNase L by degrading 2-5A. J Interferon Cytokine Res **34:**455–463. http://dx.doi.org/10.1089/jir.2014.0007.
22. **Stark GR, Kerr IM, Williams BR, Silverman RH, Schreiber RD.** 1998. How cells respond to interferons. Annu Rev Biochem **67:**227–264. http://dx.doi.org/10.1146/annurev.biochem.67.1.227.
23. **Castelli J, Wood KA, Youle RJ.** 1998. The 2-5A system in viral infection and apoptosis. Biomed Pharmacother **52:**386–390. http://dx.doi.org/10.1016/S0753-3322(99)80006-7.
24. **Castelli JC, Hassel BA, Maran A, Paranjape J, Hewitt JA, Li XL, Hsu YT, Silverman RH, Youle RJ.** 1998. The role of 2′-5′ oligoadenylate-activated ribonuclease L in apoptosis. Cell Death Differ **5:**313–320. http://dx.doi.org/10.1038/sj.cdd.4400352.
25. **Zhao L, Jha BK, Wu A, Elliott R, Ziebuhr J, Gorbalenya AE, Silverman RH, Weiss SR.** 2012. Antagonism of the interferon-induced OAS-RNase L pathway by murine coronavirus ns2 protein is required for virus replication and liver pathology. Cell Host Microbe **11:**607–616. http://dx.doi.org/10.1016/j.chom.2012.04.011.
26. **Sorgeloos F, Jha BK, Silverman RH, Michiels T.** 2013. Evasion of antiviral innate immunity by Theiler's virus L* protein through direct inhibition of RNase L. PLoS Pathog **9:**e1003474. http://dx.doi.org/10.1371/journal.ppat.1003474.
27. **Randall RE, Goodbourn S.** 2008. Interferons and viruses: an interplay between induction, signalling, antiviral responses and virus countermeasures. J Gen Virol **89:**1–47. http://dx.doi.org/10.1099/vir.0.83391-0.
28. **Han JQ, Townsend HL, Jha BK, Paranjape JM, Silverman RH, Barton DJ.** 2007. A phylogenetically conserved RNA structure in the poliovirus open reading frame inhibits the antiviral endoribonuclease RNase L. J Virol **81:**5561–5572. http://dx.doi.org/10.1128/JVI.01857-06.
29. **Zhao L, Birdwell LD, Wu A, Elliott R, Rose KM, Phillips JM, Li Y, Grinspan J, Silverman RH, Weiss SR.** 2013. Cell-type-specific activation of the oligoadenylate synthetase-RNase L pathway by a murine coronavirus. J Virol **87:**8408–8418. http://dx.doi.org/10.1128/JVI.00769-13.
30. **Taniguchi T, Takaoka A.** 2001. A weak signal for strong responses: interferon-alpha/beta revisited. Nat Rev Mol Cell Biol **2:**378–386. http://dx.doi.org/10.1038/35073080.
31. **Sato M, Taniguchi T, Tanaka N.** 2001. The interferon system and interferon regulatory factor transcription factors: studies from gene knockout mice. Cytokine Growth Factor Rev **12:**133–142. http://dx.doi.org/10.1016/S1359-6101(00)00032-0.
32. **Gombold JL, Hingley ST, Weiss SR.** 1993. Fusion-defective mutants of mouse hepatitis virus A59 contain a mutation in the spike protein cleavage signal. J Virol **67:**4504–4512.
33. **Zhou A, Paranjape JM, Hassel BA, Nie H, Shah S, Galinski B, Silverman RH.** 1998. Impact of RNase L overexpression on viral and cellular growth and death. J Interferon Cytokine Res **18:**953–961.
34. **Roth-Cross JK, Stokes H, Chang G, Chua MM, Thiel V, Weiss SR, Gorbalenya AE, Siddell SG.** 2009. Organ-specific attenuation of murine hepatitis virus strain A59 by replacement of catalytic residues in the putative viral cyclic phosphodiesterase ns2. J Virol **83:**3743–3753. http://dx.doi.org/10.1128/JVI.02203-08.
35. **Park MS, Shaw ML, Munoz-Jordan J, Cros JF, Nakaya T, Bouvier N, Palese P, Garcia-Sastre A, Basler CF.** 2003. Newcastle disease virus (NDV)-based assay demonstrates interferon-antagonist activity for the NDV V protein and the Nipah virus V, W, and C proteins. J Virol **77:**1501–1511. http://dx.doi.org/10.1128/JVI.77.2.1501-1511.2003.
36. **Gitlin L, Barchet W, Gilfillan S, Cella M, Beutler B, Flavell RA, Diamond MS, Colonna M.** 2006. Essential role of mda-5 in type I IFN responses to polyriboinosinic:polyribocytidylic acid and encephalomyocarditis picornavirus. Proc Natl Acad Sci U S A **103:**8459–8464. http://dx.doi.org/10.1073/pnas.0603082103.
37. **Pinto AK, Daffis S, Brien JD, Gainey MD, Yokoyama WM, Sheehan KC, Murphy KM, Schreiber RD, Diamond MS.** 2011. A temporal role of type I interferon signaling in CD8+ T cell maturation during acute West Nile virus infection. PLoS Pathog **7:**e1002407. http://dx.doi.org/10.1371/journal.ppat.1002407.
38. **Casson CN, Copenhaver AM, Zwack EE, Nguyen HT, Strowig T, Javdan B, Bradley WP, Fung TC, Flavell RA, Brodsky IE, Shin S.** 2013. Caspase-11 activation in response to bacterial secretion systems that access the host cytosol. PLoS Pathog **9:**e1003400. http://dx.doi.org/10.1371/journal.ppat.1003400.
39. **Caamano J, Alexander J, Craig L, Bravo R, Hunter CA.** 1999. The NF-kappa B family member RelB is required for innate and adaptive immunity to Toxoplasma gondii. J Immunol **163:**4453–4461.
40. **Inaba K, Inaba M, Romani N, Aya H, Deguchi M, Ikehara S, Muramatsu S, Steinman RM.** 1992. Generation of large numbers of dendritic cells from mouse bone marrow cultures supplemented with granulocyte/macrophage colony-stimulating factor. J Exp Med **176:**1693–1702. http://dx.doi.org/10.1084/jem.176.6.1693.
41. **Copenhaver AM, Casson CN, Nguyen HT, Fung TC, Duda MM, Roy CR, Shin S.** 2014. Alveolar macrophages and neutrophils are the primary reservoirs for Legionella pneumophila and mediate cytosolic surveillance of type IV secretion. Infect Immun **82:**4325–4336. http://dx.doi.org/10.1128/IAI.01891-14.
42. **Bender SJ, Phillips JM, Scott EP, Weiss SR.** 2010. Murine coronavirus receptors are differentially expressed in the central nervous system and play virus strain-dependent roles in neuronal spread. J Virol **84:**11030–11044. http://dx.doi.org/10.1128/JVI.02688-09.
43. **Sheehan KC, Lai KS, Dunn GP, Bruce AT, Diamond MS, Heutel JD, Dungo-Arthur C, Carrero JA, White JM, Hertzog PJ, Schreiber RD.** 2006. Blocking monoclonal antibodies specific for mouse IFN-alpha/beta receptor subunit 1 (IFNAR-1) from mice immunized by in vivo hydrodynamic transfection. J Interferon Cytokine Res **26:**804–819. http://dx.doi.org/10.1089/jir.2006.26.804.
44. **Xiang Y, Wang Z, Murakami J, Plummer S, Klein EA, Carpten JD, Trent JM, Isaacs WB, Casey G, Silverman RH.** 2003. Effects of RNase L

mutations associated with prostate cancer on apoptosis induced by 2′,5′-oligoadenylates. Cancer Res **63:**6795–6801.
45. **Schroeder A, Mueller O, Stocker S, Salowsky R, Leiber M, Gassmann M, Lightfoot S, Menzel W, Granzow M, Ragg T.** 2006. The RIN: an RNA integrity number for assigning integrity values to RNA measurements. BMC Mol Biol **7:**3. http://dx.doi.org/10.1186/1471-2199-7-3.
46. **Zhou Y, Kang MJ, Jha BK, Silverman RH, Lee CG, Elias JA.** 2013. Role of ribonuclease L in viral pathogen-associated molecular pattern/influenza virus and cigarette smoke-induced inflammation and remodeling. J Immunol **191:**2637–2646. http://dx.doi.org/10.4049/jimmunol.1300082.
47. **Knijnenburg TA, Roda O, Wan Y, Nolan GP, Aitchison JD, Shmulevich I.** 2011. A regression model approach to enable cell morphology correction in high-throughput flow cytometry. Mol Syst Biol **7:**531. http://dx.doi.org/10.1038/msb.2011.64.
48. **Cooper DA, Banerjee S, Chakrabarti A, Garcia-Sastre A, Hesselberth JR, Silverman RH, Barton DJ.** 2015. RNase L targets distinct sites in influenza A virus RNAs. J Virol **89:**2764–2776. http://dx.doi.org/10.1128/JVI.02953-14.
49. **Roth-Cross JK, Martinez-Sobrido L, Scott EP, Garcia-Sastre A, Weiss SR.** 2007. Inhibition of the alpha/beta interferon response by mouse hepatitis virus at multiple levels. J Virol **81:**7189–7199. http://dx.doi.org/10.1128/JVI.00013-07.
50. **Gough DJ, Messina NL, Clarke CJ, Johnstone RW, Levy DE.** 2012. Constitutive type I interferon modulates homeostatic balance through tonic signaling. Immunity **36:**166–174. http://dx.doi.org/10.1016/j.immuni.2012.01.011.
51. **Sato M, Suemori H, Hata N, Asagiri M, Ogasawara K, Nakao K, Nakaya T, Katsuki M, Noguchi S, Tanaka N, Taniguchi T.** 2000. Distinct and essential roles of transcription factors IRF-3 and IRF-7 in response to viruses for IFN-alpha/beta gene induction. Immunity **13:**539–548. http://dx.doi.org/10.1016/S1074-7613(00)00053-4.
52. **Lazear HM, Pinto AK, Vogt MR, Gale M, Jr, Diamond MS.** 2011. Beta interferon controls West Nile virus infection and pathogenesis in mice. J Virol **85:**7186–7194. http://dx.doi.org/10.1128/JVI.00396-11.
53. **Fenner JE, Starr R, Cornish AL, Zhang JG, Metcalf D, Schreiber RD, Sheehan K, Hilton DJ, Alexander WS, Hertzog PJ.** 2006. Suppressor of cytokine signaling 1 regulates the immune response to infection by a unique inhibition of type I interferon activity. Nat Immunol **7:**33–39. http://dx.doi.org/10.1038/ni1287.
54. **Samuel MA, Whitby K, Keller BC, Marri A, Barchet W, Williams BR, Silverman RH, Gale M, Jr, Diamond MS.** 2006. PKR and RNase L contribute to protection against lethal West Nile Virus infection by controlling early viral spread in the periphery and replication in neurons. J Virol **80:**7009–7019. http://dx.doi.org/10.1128/JVI.00489-06.
55. **Chan RW, Chan MC, Agnihothram S, Chan LL, Kuok DI, Fong JH, Guan Y, Poon LL, Baric RS, Nicholls JM, Peiris JS.** 2013. Tropism of and innate immune responses to the novel human betacoronavirus lineage C virus in human ex vivo respiratory organ cultures. J Virol **87:**6604–6614. http://dx.doi.org/10.1128/JVI.00009-13.
56. **Spiegel M, Pichlmair A, Martinez-Sobrido L, Cros J, Garcia-Sastre A, Haller O, Weber F.** 2005. Inhibition of beta interferon induction by severe acute respiratory syndrome coronavirus suggests a two-step model for activation of interferon regulatory factor 3. J Virol **79:**2079–2086. http://dx.doi.org/10.1128/JVI.79.4.2079-2086.2005.
57. **Versteeg GA, Bredenbeek PJ, van den Worm SH, Spaan WJ.** 2007. Group 2 coronaviruses prevent immediate early interferon induction by protection of viral RNA from host cell recognition. Virology **361:**18–26. http://dx.doi.org/10.1016/j.virol.2007.01.020.
58. **Kindler E, Jonsdottir HR, Muth D, Hamming OJ, Hartmann R, Rodriguez R, Geffers R, Fouchier RA, Drosten C, Muller MA, Dijkman R, Thiel V.** 2013. Efficient replication of the novel human betacoronavirus EMC on primary human epithelium highlights its zoonotic potential. mBio **4:**e00611–00612. http://dx.doi.org/10.1128/mBio.00611-12.
59. **Chan JF, Chan KH, Choi GK, To KK, Tse H, Cai JP, Yeung ML, Cheng VC, Chen H, Che XY, Lau SK, Woo PC, Yuen KY.** 2013. Differential cell line susceptibility to the emerging novel human betacoronavirus 2c EMC/2012: implications for disease pathogenesis and clinical manifestation. J Infect Dis **207:**1743–1752. http://dx.doi.org/10.1093/infdis/jit123.
60. **Zielecki F, Weber M, Eickmann M, Spiegelberg L, Zaki AM, Matrosovich M, Becker S, Weber F.** 2013. Human cell tropism and innate immune system interactions of human respiratory coronavirus EMC compared to those of severe acute respiratory syndrome coronavirus. J Virol **87:**5300–5304. http://dx.doi.org/10.1128/JVI.03496-12.
61. **Trinchieri G.** 2010. Type I interferon: friend or foe? J Exp Med **207:**2053–2063. http://dx.doi.org/10.1084/jem.20101664.
62. **de Visser KE, Eichten A, Coussens LM.** 2006. Paradoxical roles of the immune system during cancer development. Nat Rev Cancer **6:**24–37. http://dx.doi.org/10.1038/nrc1782.
63. **Hata N, Sato M, Takaoka A, Asagiri M, Tanaka N, Taniguchi T.** 2001. Constitutive IFN-alpha/beta signal for efficient IFN-alpha/beta gene induction by virus. Biochem Biophys Res Commun **285:**518–525. http://dx.doi.org/10.1006/bbrc.2001.5159.
64. **Harada H, Fujita T, Miyamoto M, Kimura Y, Maruyama M, Furia A, Miyata T, Taniguchi T.** 1989. Structurally similar but functionally distinct factors, IRF-1 and IRF-2, bind to the same regulatory elements of IFN and IFN-inducible genes. Cell **58:**729–739. http://dx.doi.org/10.1016/0092-8674(89)90107-4.
65. **Taniguchi T, Ogasawara K, Takaoka A, Tanaka N.** 2001. IRF family of transcription factors as regulators of host defense. Annu Rev Immunol **19:**623–655. http://dx.doi.org/10.1146/annurev.immunol.19.1.623.
66. **Lubick KJ, Robertson SJ, McNally KL, Freedman BA, Rasmussen AL, Taylor RT, Walts AD, Tsuruda S, Sakai M, Ishizuka M, Boer EF, Foster EC, Chiramel AI, Addison CB, Green R, Kastner DL, Katze MG, Holland SM, Forlino A, Freeman AF, Boehm M, Yoshii K, Best SM.** 2015. Flavivirus antagonism of type I interferon signaling reveals prolidase as a regulator of IFNAR1 surface expression. Cell Host Microbe **18:**61–74. http://dx.doi.org/10.1016/j.chom.2015.06.007.
67. **Zurney J, Howard KE, Sherry B.** 2007. Basal expression levels of IFNAR and Jak-STAT components are determinants of cell-type-specific differences in cardiac antiviral responses. J Virol **81:**13668–13680. http://dx.doi.org/10.1128/JVI.01172-07.